Fracture Mechanics of Concrete and Concrete Structures - Recent Advances in Fracture Mechanics of Concrete - B. H. Oh, et al.(eds)

The response of concrete structure under dynamic loadings: tools for seismic effects and impacts

J. Mazars
Structures – Risques – Grenoble University, BP 53, 38041 Grenoble, France
A. Rouquand & C. Pontiroli
Centre d'Etudes de Gramat, BP 80200, 46500 Gramat, France

ABSTRACT: The causes of the non linear behavior of concrete until failure are numerous and complex, particularly for non monotonic and rapid loadings. We present here a model coupling damage and plasticity including several effects: development and closure of cracks, damping, compaction, strain rate effects, ... The idea being to describe with the same tool a wide variety of problems, the model is of explicit form, what makes possible its implementation into explicit numerical scheme well adapted to the treatment of fast dynamic problems. In this context the F.E. "Abaqus explicit" code is used and the model has been successfully applied during the past few years to model a large range of complex reinforced concrete structures subjected to severe loadings. In this paper the main model concepts are presented and some examples of numerical simulations are given and compared to experimental data. The applications proposed in this paper are mainly related to seismic loading and to impact. The results show the relevance of the modeling used, which really allows making some real numerical experiments very useful for complex structures and extreme loadings.

1 INTRODUCTION

The simulation of the failure process of reinforced structures submitted to severe loading is still a challenge. Several physical phenomena should be considered. Damage and cracking are the main phenomena for classical loadings. However, for earthquake or impacts, high strain rate and damping play a major role. In addition, for high velocity impacts high pressure occurs locally.

Such phenomena generate pore collapse mechanisms that dissipate a large amount of energy. In the same time, at some distance from the projectile, the physical phenomena change progressively to become structure oscillations at moderate strain rate levels. The material response is now driven by an increase of concrete damage due to crack opening mechanisms, crack closure effects, and friction phenomena related to differential displacements at the crack tip level.

The material model should account for all of the consequences of these effects such as stiffness deterioration, recovery of stiffness due to crack closure, permanent strains and frictional stresses that generate hysteretic loops during unloading and reloading paths. All these mechanisms should be implemented together in a unique material model able to simulate a large range of static and dynamic problems.

Different kinds of models are proposed to simulate the behavior of concrete structures, including plasticity (Ottosen 1979), damage (Mazars 1986, Mazars & Pijaudier-Cabot 1989, La Borderie et al. 1994, Jirasek 2004, Gatuingt et al. 2008) or fracture-based approaches (Bazant 1994). Nevertheless, very few are able to simulate both phenomena.

The ability of the constitutive model to reproduce the real material behavior is not the only challenge. Numerical aspects, related to the algorithm used to compute in a finite element analysis, the stress tensor, the damage areas at the local level, or the computation of structural displacements at the global level are also very important. At each level, the computational procedure has to be numerically efficient and robust.

After presenting the model set up (PRM coupled model), applications are shown at the material level related to high confinement and at the structural level related to seismic and impact loadings. Finite element results are compared to experimental data showing the relevance of the modeling.

2 BEHAVIOUR OF CONCRETE UNDER VARIOUS LOADING

It has been shown (Mazars 1986) that, for local micro cracking, three different damage modes have to be considered:

A/ situation dominated by mode I, related to local extension ($\varepsilon_i > 0$),

B/ situation dominated by mode II (or/and III) without any local extension,

C/ situation related to the application of a strong hydrostatic pressure which leads to compaction (pore collapse in the cement matrix).

Most of concrete models are adapted to simulate the situation "A", often present in classical reinforced concrete structures. For severe loadings, related to natural (earthquake, rock fall) or technological hazards (accidental or intentional actions) two further aspects must be considered: the dynamic nature of the loading and locally, high confinement pressure. However very few models are able to simulate both phenomena. To model the behaviors which arise, the strategy is the coupling of a damage model and a plasticity model including compaction effects.

2.1 *Scalar damage model (PRM model)*

2.1.1 *Constitutive relations*

To simulate the behavior of concrete at a moderate stress level, a two scalar damage model has been proposed from works by J. Mazars (1986), C. Pontiroli (1995) and A. Rouquand (1995 & 2005). This model, named "PRM model", simulates the cyclic behavior of concrete for low confinement (type A introduced before).

This model distinguishes the behavior under traction and the behavior under compression. Between these two loading states a transition zone is defined by (σ_{ft}, ε_{ft}), where σ_{ft} and ε_{ft} are the crack closure stress and the crack closure strain respectively. The main constitutive equations of the PRM model for a uniaxial loading are the following.

For traction:

$$(\sigma - \sigma_{ft}) = E_0 \cdot (1-D_t) \cdot (\varepsilon-\varepsilon_{ft}) \qquad (1)$$

For compression:

$$(\sigma - \sigma_{ft}) = E_0 \cdot (1-D_c) \cdot (\varepsilon-\varepsilon_{ft}) \qquad (2)$$

E_0 is the initial Young's modulus; D_t and D_c are the damage variables, for traction and compression respectively. The equivalent strain $\tilde{\varepsilon} = \sqrt{\sum_i \langle x_i \rangle_+^2}$ (Mazars 1986), drives the damage evolutions; $\langle x_i \rangle_+ = x_i$ if $x_i > 0$ and $\langle x_i \rangle_+ = 0$ if not. Depending on the sign of the stress in the direction i : $x_i = \varepsilon_i$ in compression and $x_i = (\varepsilon - \varepsilon_{ft})_i$ in traction. The general evolution of damage is of exponential shape, driven by $\tilde{\varepsilon}$: $D_t = f_t(\tilde{\varepsilon}, \varepsilon_{0t}, A_t, B_t)$ and $D_c = f_c(\tilde{\varepsilon}, \varepsilon_{0c}, A_c, B_c)$. A_t, B_t, A_c, B_c are material parameters; ε_{0t} , ε_{0c} are respectively the tensile and compressive damage threshold.

Before any damage in compression, $\varepsilon_{ft} = \varepsilon_{ft0}$ (material parameter), afterwards ε_{ft} is directly linked to D_c. The transition between the two kinds of damage is located at (σ_{ft}, ε_{ft}). Figure 1 illustrates the corresponding response for a uniaxial cyclic loading.

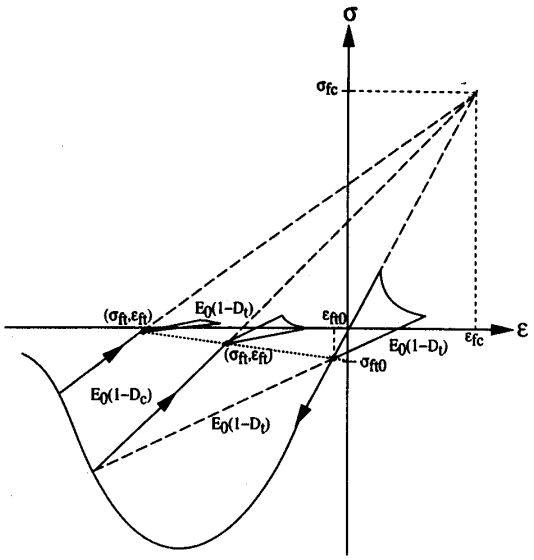

Figure 1. PRM model: stress-strain curve for a tension - compression loading path.

One can observe that the behavior can be described by the classical equation:

$$\sigma_d = E_0 (1-D_i) \varepsilon_d \qquad (3)$$

with Di = Dt or Dc ; $\varepsilon_d = \varepsilon - \varepsilon_{ft}$ and $\sigma_d = \sigma - \sigma_{ft}$

In the framework of isotropic damage evolutions (D is a scalar), the general 3D constitutive equations of the model relating strain and stress tensors (in bold) is:

$$\boldsymbol{\sigma}_d = \boldsymbol{\Lambda}_0 (1-D) \boldsymbol{\varepsilon}_d \quad \text{or} \qquad (4)$$

$$(\boldsymbol{\sigma} - \boldsymbol{\sigma}_{ft}) = (1-D) [\lambda_0 \, \mathrm{Tr}(\boldsymbol{\varepsilon} - \boldsymbol{\varepsilon}_{ft}) 1 + 2\mu_0 (\boldsymbol{\varepsilon} - \boldsymbol{\varepsilon}_{ft})]$$

where $\boldsymbol{\sigma}_{ft}$ and $\boldsymbol{\varepsilon}_{ft}$ are respectively the crack closure stress and strain tensors used to manage permanent effects; $\boldsymbol{\Lambda}_0$ is related to the initial mechanical characteristics of the material. Damage D remains a scalar and is issued from a combination of the two modes of damage, depending of the local stress state:

$$D = \alpha_t D_t + (1- \alpha_t) D_c \qquad (5)$$

α_t evolves between 0 and 1 and the actual values depend on the sign of Tr ($\boldsymbol{\varepsilon} - \boldsymbol{\varepsilon}_{ft}$).

This formulation is an explicit one, for more details see (Mazars 1986, Rouquand & Pontiroli 1995, Rouquand 2005, Mazars et al. 2010).

2.1.2 *Strain rate effects - Internal friction, damping*

It is well known that concrete is strain rate dependent, particularly under tensile loading. This effect is accounted for using dynamic thresholds (ε_{0t}^{d} and ε_{0c}^{d}) instead of static one's (ε_{0t}^{s} and ε_{0c}^{s}) through the use of a dynamic increase factor $R = \varepsilon_0^d / \varepsilon_0^s$.

Its value for a compressive dynamic loading takes the following form:

$$R_c = \min(1.0 + a_c \dot{\varepsilon}^{b_c},\ 2.50) \tag{6}$$

and for a dynamic tensile loading:

$$R_t = \min\left[\max\left(1.0 + a_t \dot{\varepsilon}^{b_t},\ 0.9\dot{\varepsilon}^{0.46}\right),\ 10.0\right] \tag{7}$$

a_c, b_c and a_t, b_t are material coefficients identified from experimental results. For a high strain rate, the tensile dynamic increase factor is supposed to follow an empirical formula ($0.9\dot{\varepsilon}^{0.46}$) that well agrees with the experimental data obtained by Brara & Klepaczko (1999) using a Hopkinson bar. These results have been obtained on ordinary micro concrete (necessary due to the size of the specimen tested). Looking forward new results it is assumed that the same trend can be used for the concrete considered here after.

For cyclic loading, as the one encountered during an earthquake loading, friction stresses induce significant dissipated energy during unloading and reloading cycles. To account for this important phenomenon, an additional damping stress is introduced in the model:

$$\boldsymbol{\sigma} - \boldsymbol{\sigma}_{ft} = (\boldsymbol{\sigma} - \boldsymbol{\sigma}_{ft})^{\text{damage}} + \boldsymbol{\sigma}^{\text{damping}} \tag{8}$$

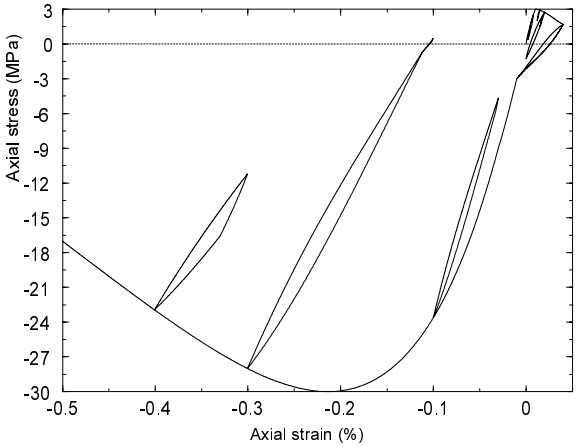

Figure 2. PRM model: uniaxial cyclic loading including damping stress.

The damping stress generates a hysteretic loop during the unloading and the reloading cycle. This stress is calculated from the damping ratio ξ, classically defined as the ratio between the area under the closed loop and the area under the linear elastic-damage stress curve, which gives for the uniaxial case:

$$\xi = \frac{A_h}{E_0(1-D)\left(\varepsilon_{\max} - \varepsilon_{ft}\right)^2} \tag{9}$$

A_h is the loop area under the stress strain curve, $E_0(1\text{-}D)$ is the current material stiffness. ε_{max} is the maximum strain before unloading; ε_{ft} is the closure strain that defines the transition point between compression and tension as seen before. From (9) it can be shown that the damping ratio ξ is related to damage D according to the relation:

$$\xi = (\beta_1 + \beta_2 D) \tag{10}$$

β_1 is a damping ratio for an undamaged and perfectly elastic material. $\beta_1 + \beta_2$ is the damping ratio for a fully damaged material. Usually β_1 can be chosen equal to 0.02 and β_2 can be chosen equal to 0.05. Figure 2 shows, for cyclic tensile or compressive loading, the strain stress curve including damping stresses.

2.2 *Elasto-plastic model – PRM coupled model*

The previous damage model is very efficient to simulate the behavior of concrete for unconfined or low confined cyclic loading (Rouquand 2005). For very high dynamic loads leading to a higher pressure level, an elasto-plastic model is more appropriate. For example, the impact of a projectile striking a concrete plate at 300m/s induces local pressures near the projectile nozzle of several hundred MPa, which induces a combination of type B and C modes seen before. The previous damage model can neither simulate the pore collapse phenomena nor the shear plastic strain occurring in this pressure level. To overcome these limitations, the elasto-plastic model proposed by Krieg (1978), for geologic materials has been chosen to simulate this kind of problem. From this simple elasto-plastic model, an improvement has been introduced in order to take into account the non linear elastic behavior encountered during an unloading and reloading cycle under a high pressure level. Another recent improvement (not presented here) has been done to take into account the water content effects, introducing an effective stress theory as described by C. Mariotti (2002). This effect induces changes on the pressure volume curve and on the shear plastic stress limit. Finally both models have been coupled to simulate the combination of the three types of situations (A, B, C) seen before.

2.2.1 *The modified Krieg model*

The Krieg model can be applied to describe the behavior of a dry material. It is based on a classical elastic - purely plastic description using a parabolic deviatoric plastic threshold including a cut-off linked to the porosity of the material and to the water content (Fig. 4):

$$q = \min\left(q_0 = \sqrt{a_0 + a_1 P + a_2 P^2}\ ,\ q_{max}\right),$$

$$\text{with } q = (3/2\ \boldsymbol{\sigma}^{\mathbf{d}} : \boldsymbol{\sigma}^{\mathbf{d}})^{1/2} \quad \text{(Von Mises stress)} \quad (11)$$

The stress tensor being $\boldsymbol{\sigma} = -P\ \mathbf{1} + \boldsymbol{\sigma}^{\mathbf{d}}$, P is the pressure of confinement and $\boldsymbol{\sigma}^{\mathbf{d}}$ is the deviatoric stress tensor.

The improvements made here concern the elastic behavior which is non linear and pressure dependent. This non linearity increases as the pore collapse phenomenon progresses. Figure 3 shows a typical P-ε_v curve used in the modified Krieg model (ε_v = trace[ε], is the volumic deformation). For pressure values lower than P_1, the behavior between pressure and volume is linear and elastic. For a pressure greater than P_1, the pore collapse mechanism becomes effective. During the loading process the pressure-volume response follows a curve identified from experiments. During the unloading, the behavior is elastic and non linear. The bulk modulus becomes pressure dependent. It is equal to K_{max} at the first unloading point and decreases to K_{min} when the tensile pressure cut-off P_{min} is reached (this value is generally negative. This pressure cut-off becomes smaller and smaller as the maximum pressure P_{max} increases. When P_{max} is close to P_1, K_{max} is close to K_{min} and also close to the initial bulk modulus K_p. When P_{max} reaches P_{cons}, K_{max} becomes equal to K_{grain} and K_{min} becomes equal to K_{0grain}. So the non linearity becomes more and more important as the pore collapse phenomena progresses.

When P_{max} becomes greater than P_{cons}, the pore collapse phenomena is achieved because all the voids are removed from the material. At this pressure level the material is consolidated and the behavior becomes purely elastic and non linear.

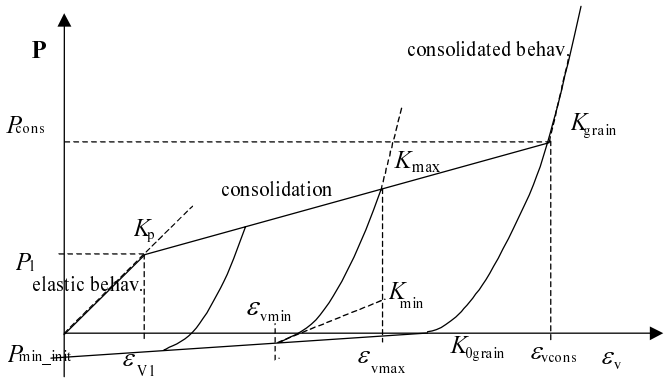

Figure 3. Krieg modified model : pressure - volumic strain behavior (P and ε_v are considered positive for compression).

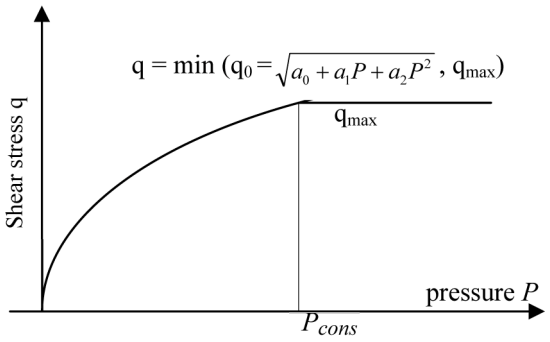

Figure 4. Krieg modified model : shear yield threshold.

2.2.2 *Coupling of damage and plasticity models*

The PRM damage model has been coupled with the modified Krieg model to give the PRM coupled model. The coupling procedure ensures a perfect continuity between the two model responses. The damage model is activated if the maximum pressure is too low to start the pore collapse phenomenon or if the shear stress is too low to reach the shear yield stress. If not, the plastic model is the one activated and it drives the evolutions until the extensions sufficiently increase to lead to a damage failure as shown in the example below (Fig. 6). The coupled model has been implemented in Abaqus explicit (Hibbitt et al. 2004) and to avoid mesh dependency the Hillerborg regularization method is used (Hillerborg 1976). This method insures a constant fracture energy (G_f) whatever is the size of finite elements.

2.2.3 *Ability of the model to simulate various loading situations*

For the damage part of the model, materials parameters are calibrated from uniaxial tests (traction and compression) and from existing data base for strain rate effects and damping.

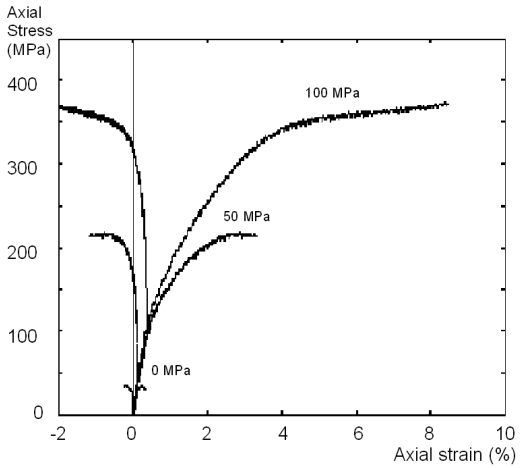

Figure 5. Experimental response of concrete subjected to triaxial compression for various confinements (Gabet et al. 2008).

The identification of the modified Krieg model needs very specific tests (hydrostatic tests at high confinement and series of triaxial tests to fit the shear yield threshold). The GIGA machine at 3S-R Grenoble allows to perform triaxial tests on cylindri-

cal samples (Φ = 7 cm, h = 14 cm) with a confining pressure capability up to 1 GPa (Gabet et al. 2008, Vu et al. 2009). GIGA is used to identify the materials parameter but also to validate the model from tri-axial specific loading paths. Figures 5 (experiment) and 6 (model) show the static response obtained on a cylindrical specimen for tri-axial tests with increasing lateral pressure. The response of the model is globally good. It exhibits the activation of the damage part for low confinement, the plasticity part for high confinement (visible when there is a plateau), a combination of both in between and the reactivation of damage when failure occurs.

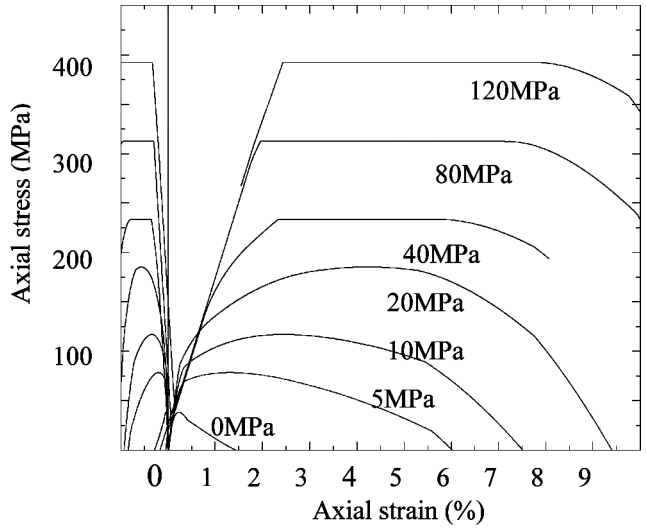

Figure 6. Response of the PRM coupled model for triaxial compression at various confinements.

3 APPLICATION TO REINFORCED CONCRETE STRUCTURES

The PRM coupled model implemented in the Abaqus explicit finite element code has been extensively used to simulate a lot of complex problems. The PRM damage part can be used with most of the available finite elements: 1D truss elements, beam elements, 2D plane stress and plane strain elements, 2D axisymmetric elements, shell elements, 3D solid elements, etc. The PRM coupled model can be used with 2D plane strain elements, 2D axisymmetric and 3D solid elements. In order to show the abilities of the coupled model some applications on reinforced concrete structures are presented below and numerical results are compared to experimental data.

3.1 *Structural walls submitted to earthquake*

In this example we compare numerical (Rouquand 2001) and experimental results (Combescure et al. 2000), obtained on a mock-up (1/3rd scale, 5 storeys, 33 tons) composed of 2 reinforced concrete structural walls and tested on the shaking table at CEA in Saclay - France. This experimental work has been done in the framework of the French CAMUS research program performed to defend the seismic French rules to design structural walls with a few ratio of reinforcement. In order to prescribe the correct gravity load obtained on the full scale building, additional masses are introduced on the reduced scale specimen at each floor level. The footprints of the tested reinforced concrete structure are rigidly linked to the table. All the details of the structure (geometric data, reinforcement data, material parameters, etc.) can be found on (Rouquand 2001) or (Combescure et al. 2000 and Combescure, Mazars et al. 2001). Figure 7 shows a general view of the mock-up and two of the different finite element meshes used in the numerical simulations. The first finite element mesh is a 2D model with a regular mesh size. The second one is a 3D mesh and the finite element size is reduced by two, in comparison with the first one.

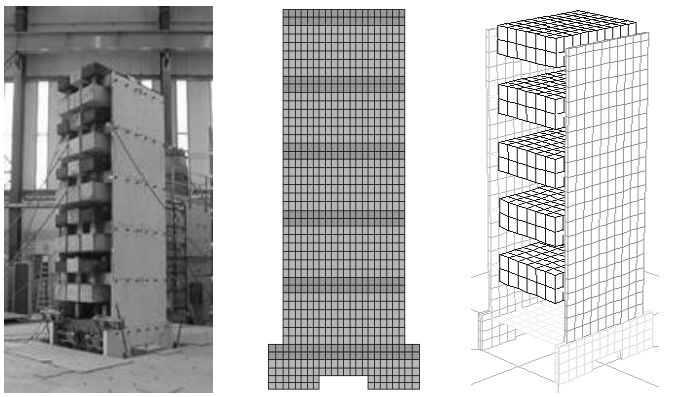

Figure 7. General view of the mock-up and the two kinds of finite element models, 2D and 3D.

A series of increasing earthquake loading is applied to the specimen. The prescribed acceleration profiles are generated in the horizontal direction belonging to the structural wall planes. Figure 8 shows the acceleration profile imposed to the shaking table. The first earthquake, Nice 0.22g, is representative of a far field seismic load with a peak ground acceleration (pga) of 0.22g (g = 9.81 m/s^2). Melendy ranch corresponds to a near field earthquake with a pga of 1.35g. Nice 0.64g and Nice 1.0g are far field earthquakes with a pga of 0.64g and 1.0g respectively. The Abaqus explicit finite element code and the PRM model (here, only the damage part is activated) is used to simulate the behaviour of the structure under the four earthquake loads consecutively applied.

Figure 9 gives an example of the results obtained: the comparison between numerical and experimental displacements after the Melendy ranch loading. The plotted displacements correspond to the horizontal displacement at the top of the building (reference is the shaking table). The numerical results match very well with the measured curves, as well for the amplitude as for the frequency.

Figure 10 shows a view of the tensile damaged areas at the end of the Nice 1.0g earthquake. Numerical simulations give comparable results for the tensile damage contours which are consistent with the crack pattern raised at the end of the tests.

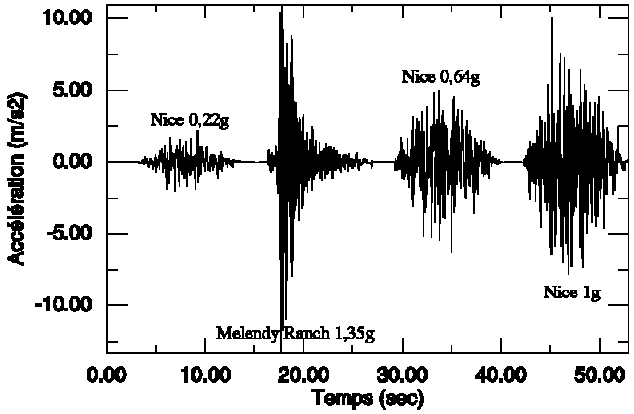

Figure 8. Acceleration profile prescribed on the building specimen.

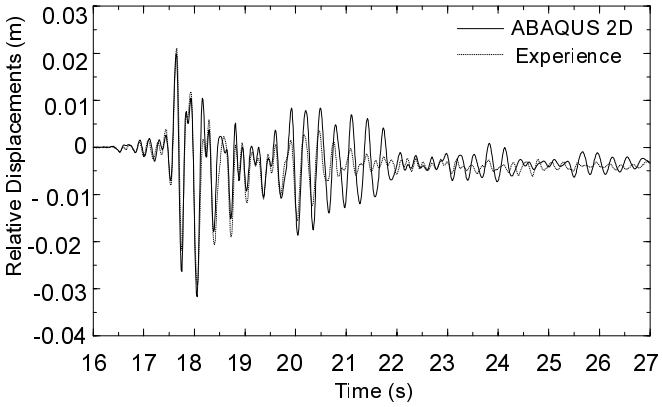

Figure 9. Comparison of predicted and measured results (Melendy ranch 1.35g).

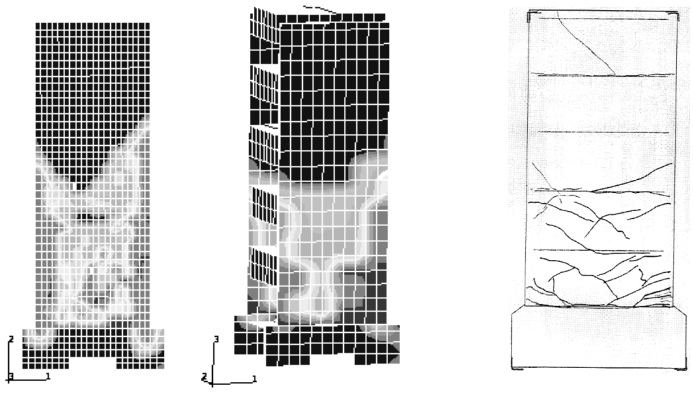

Figure 10. Predicted and measured tensile damage contours after the Nice 1.0g earthquake and the corresponding crack pattern.

It was observed that the predicted values are respectively slightly underestimated for the displacement and slightly overestimated for the forces. It seems that the mean reason of these discrepancies can be attributed to sliding effects between reinforcement and concrete in highly damaged areas. In these areas due to cyclic loading, buckling mode can be observed for the reinforcement and the numerical model assumed that the strains on concrete and on reinforcement are the same. Some improvements are needed to solve this problem.

3.2 *Impact of a soft projectile on a plate*

The problem presented here concerns the crash of a soft missile impacting a reinforced concrete structure. This kind of impact is not a very highly dynamic event but it can generate severe structural damage. Numerical simulations of this problem are not easy because there are strong interactions between the target behaviour and the missile crash behaviour. Correct predictions suppose that the response of the target and of the missile is properly modelled. In order to evaluate the capabilities of the explicit finite element code Abaqus including the PRM coupled model, 3-D numerical simulations of Meppen tests (tests n°12 and n°20 presented below) have been done (Rouquand 2006). The objective is to determine the capabilities and the limits of such simulations.

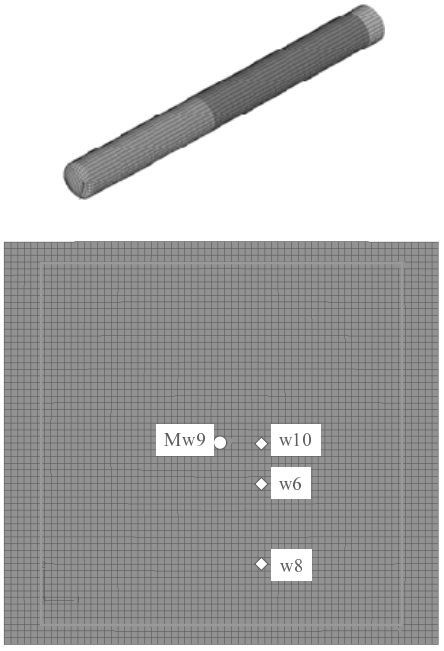

Figure 11. Mesh of the projectile and of the target with the location of the points where displacements are measured (tests n°12).

Missile impact on a reinforced concrete structure can simultaneously generate local and global damages. A 3-D finite element model with solid brick elements is the most appropriate to reproduce the local and the global complex strain field generated during the impact on the target. The projectile is composed of a thin steel tube which can be efficiently modelled using 3-D shell elements. The target size is 6.5m by 6.0m, the thickness is 70cm in test n°12 and only 50cm in test n°20 (see the scheme

for test n° 12 and test n° 20 respectively on Figs. 13-14). Figure 11 shows a view of the meshes. About 30 000 3-D solid elements are used to model the target. The reinforcement is introduced using the Abaqus rebar option. This option allows to take into account the stiffness and the mass contribution of the reinforcement in the elementary stiffness matrix and in the elementary mass matrix associated to the 3-D solid elements. The rebar definition requires the definition of the reinforcement constitutive material.

The projectile mesh is composed of about 6500 "S4R" Abaqus shell elements used for thin or moderately thick structures. This projectile is a generic missile. Its length is 6m and its diameter is 0.6m. The thickness of the steel envelop is 7mm in a first part and 10mm in the second part. An additional mass is incorporated on the rear part of the projectile to model lest.

The behaviour of the metallic bars is modelled using a standard elastic and plastic model. Strain rate is not accounted because it is very low in the reinforcement. The behaviour of the metallic missile material is modelled using the Johnson Cook (1983) elasto-plastic model. Strain rate is now accounted because during the projectile crash, it can reach about 1000/s. In the tests, the reinforced concrete slab was put on a vertical position at the end of a rail. The projectile is accelerated on the rail and impacts the plate in its middle point. The slab is supported on a very stiff metallic frame of 5.4m by 5.4m centred on its rear face. To simulate this support, all the nodes on the rear face located along the frame, are fixed (zero displacement) in the plate normal direction. The missile initial velocity is 241.5m/s in test n°12 and 197.7m/s in test n°20. The missile axis and the velocity vector are perpendicular to the reinforced concrete plate.

3.2.1 *Test n° 12*

Figure 12 shows a comparison between measured and computed displacements on three points (w10, w6 and w8 – see locations fig. 11). The agreement is good with an error less than 10 %.

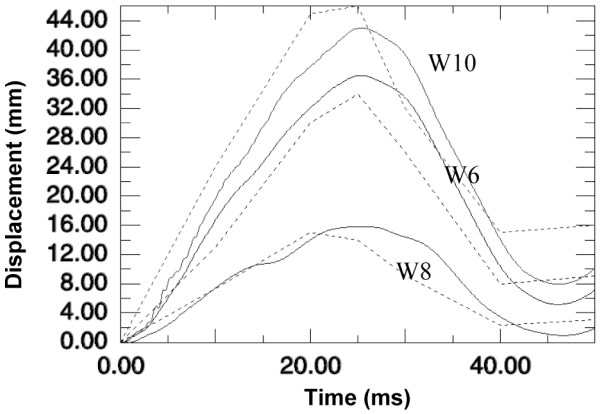

Figure 12. Comparison between measured (dashed line) and computed displacements (solid line) in test n° 12.

Figure 13 shows the comparison between the observed crack pattern and damage areas. In fact for practical reason the grey scale is related to maximum tensile strains which are directly linked to damage through the equivalent strain (see § 2.1.1). This comparison shows that the conical zone with open tensile cracks corresponds more or less to the computed cracked zone (light grey contours).

3.2.2 *Test n° 20*

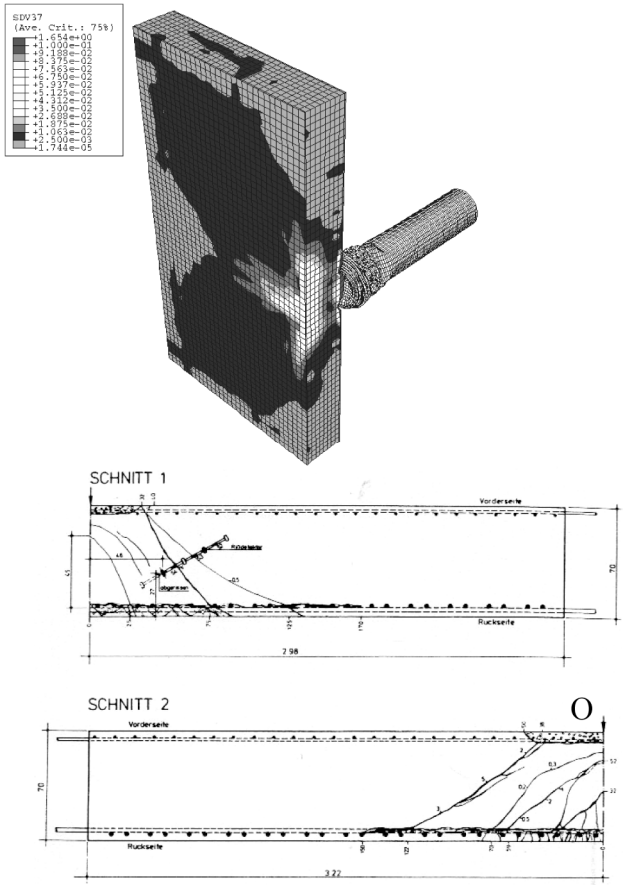

Figure 13. Comparison between computed and observed damages (test n° 12 – O is the impact location).

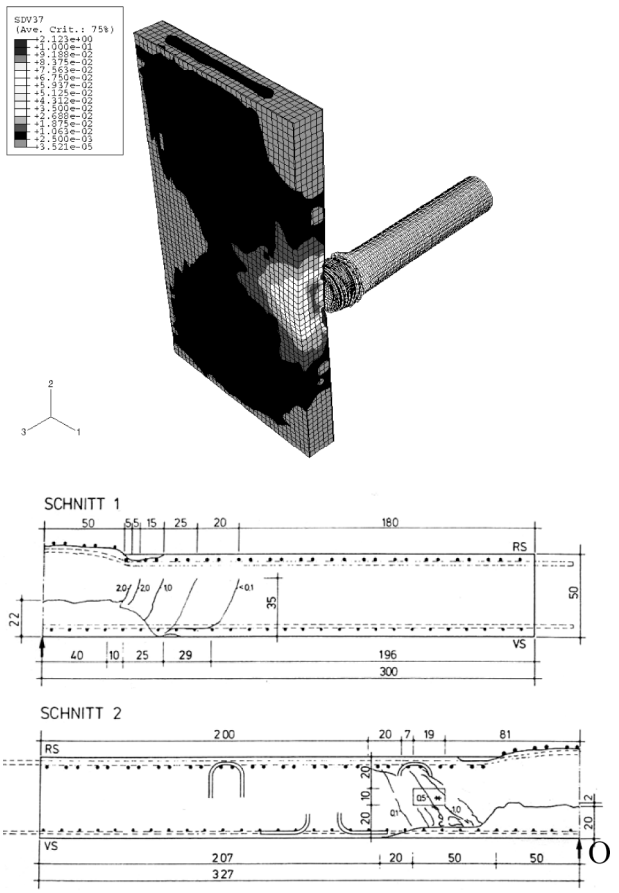

Figure 14. Comparison between computed and observed damages (test n° 20 – O is the impact location).

Figure 14 shows the comparison between the computed maximum tensile strains and the observed crack pattern (test n° 20). In this experiment severe damage is obtained in the concrete structure ahead the projectile nozzle. Because of the reduction of the slab thickness in this test, a concrete plug is now clearly observed in the experiment. This damage mode is the result of large shear strains around the plug. This kind of damage is correctly predicted in the numerical simulation.

4 CONCLUSIONS

A general constitutive model for concrete structures submitted to extreme loadings (high velocity and high confinement) has been developed and implemented into the "Abaqus explicit" finite element code in the framework of damage and plasticity mechanics. The starting point is the concrete damage model proposed by (J. Mazars 1986) for monotonic loading it was extended to treat cyclic and dynamic loading. The result is the PRM coupled model able to simulate a lot of physical mechanisms such as crack opening and crack closure effects, strain rate effects, material damping induced by internal friction, compaction of porous media, shear plastic strains under high pressure. To validate this particular coupling of plasticity and damage, an extensive experimental programme has been performed at 3S-R Grenoble using the GIGA machine which allows high confinement up to 1 GPa (Gabet et al. 2008), and a new programme is in progress on the large Hopkinson bar at JRC Ispra to complete the data base under high velocity loading.

The model implemented into the F.E. Abaqus explicit code, has been extensively used and can advantageously simulate a large range of problems going from quasi-static simulations on concrete structures to high dynamic problems related to the effect of low and high velocity impacts (Mazars et al. 2009, Rouquand et al. 2009).

The simulations presented here (seismic loading and soft impact) compared to experimental results, show the relevance of the modelling used which allows to carry out true numerical experiments very useful for complex structures and/or extreme loadings.

REFERENCES

Bazant Z.P., 1994, « Nonlocal damage theory based on micromechanic of crack interaction », *Journal of Engineering Mechanics. ASCE,* vol. 120, pp. 593-617.

Brara A., 1999, « Etude expérimentale de la traction dynamique du béton par écaillage », Thèse Univ. Metz – France.

Combescure D. et al., 2000, ICONS European program seismic tests on R/C bearing walls, CAMUS III specimen, Rapport DMT, SEMT/EMSI/RT/00-014/A, CEA Saclay, Fr.

Combescure D., Mazars J., Naze P.A. & Reynouard J.M., CAMUS III international benchmark, synthesis of participant reports, 2001, Post- Framcos-4 workshop.

Gabet, T., Malecot, Y. & Daudeville, L., 2008, "Triaxial Behavior of Concrete under High Stresses: Influence of the Loading Path on Compaction and Limit States," *Cement and Concrete Research*, V. 38, No. 3, pp. 403-412.

Gatuingt, F., Desmorat, R et al., 2008, Anisotropic 3D delay-damage model to simulate concrete structures. Revue Européenne de Mécanique Numérique. Vol 17. Pp. 740-760.

Hibbit, Karlsson & Sorense Inc, *Abaqus manuals*, version 6.4.

Hillerborg A., Modeer M. & Petersson P. E., 1976, Analysis of crack formation and growth in concrete beams of fracture mechanics and finite elements, *Cement and Concrete Research*, vol. 6, pp 773-782.

Jirásek M., 2004, « Non-local damage mechanics with application to concrete », 2004, *Revue Française de Génie Civil*, vol. 8, pp. 683-707.

Johnson, G. R. & Cook, W. H., 1983, "A Constitutive Model and Data for Letals Subjected to Large Strains, High Strain Rates and High Temperatures," *Proceedings 7th International Symposium on Ballistics*, pp. 541-547.

Krieg R. D, 1978, A simple constitutive description for soils and crushable foams », Sandia National Laboratories, SC-DR-72-0833, Albuquerque, New Mexico.

La Borderie C., Mazars et al., Pijaudier-Cabot G, 1974, Damage mechanics model for reinforced concrete structures under cyclic loading. A.C.I, 134: 147–172, 1994. edit. W.Gerstle Z.P. Bazant.

Mariotti C., Perlat J. P. & Guerin J. M., 2003, A numerical approach for partially saturated geomaterials under shock », 2002, *Intern. Jour. of Impact Eng.*, vol. 28, pp. 717 – 741.

Mazars J., 1986, A description of micro and macro scale damage of concrete structures , *Engineering Fracture Mechanics*, vol. 25, n° 5/6.

Mazars J., Pijaudier-Cabot G., 1989, Continuum damage theory - application to concrete, 1989, *Journal of Engineering Mechanics, ASCE*, vol. 115(2), pp. 345–365.

Mazars J., Rouquand A., Pontiroli C. et al. 2009, Damage tools to model severe loading effects on reinforced concrete structures, ACI SP-265, pp. 143-169.

Mazars J. et al, 2010, Concrete under various loadings : way to model in a same framework: Damage, Fracture & Compaction, keynote lecture, EURO-C 2010, Roorhmouth, Schladming, Austria

Ottosen N.S., 1979, Constitutive model for short time loading of concrete, 1979, *Journal of Engineering Mechanics, ASCE*, vol. 105, pp. 127-141.

Pontiroli C., 1995, Comportement au souffle de structures en béton armé, analyse expérimentale et modélisation, Thèse de doctorat, Ecole Normale Supérieure de Cachan - Centre d'études de Gramat.

Rouquand A., Pontiroli C., 1995, Some considerations on explicit damage models including crack closure effects and anisotropic behaviour, *Proceedings FRAMCOS-2*, Ed.F.H. Wittmann, AEDIFICATIO Publisher, Freiburg.

Rouquand A., 2002, Comportement d'un bâtiment posé sur table sismique, programme CAMUS III, comparaisons calculs expériences, Centre d'Etudes de Gramat, rapport technique T2002-00052/CEG/NC.

Rouquand A., 2005, Présentation d'un modèle de comportement des géomatériaux, applications au calcul de structures et aux effets des armes conventionnelles, Centre d'Etudes de Gramat, rapport technique T2005-00021/CEG/NC.

Rouquand A., 2006, Simulations numériques des essais Meppen : Impacts de projectiles déformables contre des parois en béton armé, Technichal report T2006-00052/CEG/NC, Centre d'Etudes de Gramat.

Rouquand A., Pontiroli C., Mazars J., 2009, Predicting concrete behaviour from quasi-static loading to hypervelocity impact: an overview of the PRM Model, EJECE journal, (submitted).

Vu, X. H., Malecot, Y., Daudeville, L. & Buzaud, E., 2009, "Experimental Analysis of Concrete Behavior under High Confinement: Effect of the Saturation Ratio," *International Journal of Solids and Structures*, 46, pp. 1105-1120.